

# Spin-mechanics with levitating ferromagnetic particles

P. Huillery<sup>1</sup>, T. Delord<sup>1</sup>, L. Nicolas<sup>1</sup>, M. Van Den Bossche<sup>1</sup>, M. Perdriat<sup>1</sup>, and G. Hétet<sup>1</sup>

<sup>1</sup>*Laboratoire de Physique de l'Ecole normale supérieure,  
ENS, Université PSL, CNRS, Sorbonne Université,  
Université Paris-Diderot, Sorbonne Paris Cité, Paris, France.*

We propose and demonstrate first steps towards schemes where the librational mode of a levitating ferromagnet is strongly coupled to the electronic spin of Nitrogen-Vacancy (NV) centers in diamond. Experimentally, we levitate ferromagnets in a Paul trap and attain oscillation frequencies in the hundreds of kHz range using homogeneous magnetic fields. These values are two orders of magnitude larger than the Paul trap librational frequencies and exceed the decoherence rate of NV centers in CVD grown diamonds. We also prepare and levitate composite diamond-ferromagnet particles and demonstrate both coherent spin control of the NV centers and read-out of the particle libration using the NV spin. Our results will find applications in ultra-sensitive gyroscopy and bring levitating objects a step closer to spin-mechanical experiments at the quantum level.

Spin-mechanical systems where electronic spins are entangled to the motion of individual atoms are now used widely for studying fundamental phenomena and for quantum information and metrological applications [1]. Inspired by the coupling schemes developed for trapped atoms [2] and single ions [3, 4], new ideas emerged to extend the field to macroscopic systems [5, 6, 8–14, 16], with perspectives to test quantum mechanics on a large scale [17].

In this direction, the NV center in diamond stands out as a promising solid state qu-bit that enables optical initialization and read-out [18] and has long spin coherence time [21, 22]. Proposals for coupling NV spins to the motion of cantilevers at the quantum level through magnetic forces [13, 22–24] or lattice strain [16, 25] have been put forward with important experimental achievements [26–33]. It has later been proposed to couple NV spins to the motion of their host diamond, levitating in a harmonic trap [8, 34]. While this allows to benefit from the very high Q-factor offered by levitating particle under vacuum [35, 36], it has also been realized that NV spins could be conveniently coupled to the librational motion (also called torsional/rotational) of the levitating diamond [9, 11] instead of the center-of-mass motion. In this direction, optical levitation experiments have shown rapid progress [38–41] but illuminated diamonds tend to warm up and escape from the trap under vacuum [42]. Paul traps [1–3, 43, 47] and magneto-gravitational traps [48] have also been implemented but, although they do not suffer as much from heating, they currently operate with lower librational frequencies [1, 3].

Here, we propose a platform for coupling spins to mechanical oscillators using the librational mode of levitating ferromagnets in a Paul trap. The proposed coupling can be achieved in the two ways that are depicted in Fig. 1. First, a diamond containing NV centers can be attached directly to the levitating ferromagnet (Fig. 1-a)). Second, the ferromagnet librational motion can be coupled to the spin of a distant NV center located in a fixed cold CVD grown nanopyramid (Fig. 1-b)), inspired by magnetic force microscopy (MRFM) [49, 50] and single spin magnetometry [27, 51] platforms. As we show

next, one of the motivations for the proposed experiments is that the librational frequency can be increased using very modest external magnetic field amplitudes and that high quality factors can be obtained with an oscillator at room temperature [35, 36]. Experimentally, we assemble and levitate micron-sized particles of soft ferromagnetic materials in a Paul trap and strongly confine their orientation magnetically. Under a magnetic field of 0.1 T, we observe librational frequencies exceeding 150 kHz and Q-factors of more than 1000 at only 1 mbar of vacuum pressure, which are promising results for high precision torque sensing. Furthermore, we trap two types of hybrid particles composed of a nano-diamond attached to a soft ferromagnet and a micro-diamond with a ferromagnetic coating. Using these composite structures with large librational confinement, we could show both efficient coherent manipulations of the NV centers's spins and spin read-out of the particle libration, which are important steps towards spin-mechanical experiments in the quantum regime.

*The levitating magnet.* At the heart of these proposals, is the levitation of ferromagnetic particles in a Paul trap (see Fig. 2a). We first levitate spherical micron-sized particles made of 98 % iron, as shown in Fig.2-b), using similar ring traps and injection technique than the ones employed to levitate micro-diamonds, described in detail in [2, 3]. Our Paul trap provide stable confinement for both the center of mass and libration of the magnet with frequencies that are typically in the kHz range. By exploiting the magnetic torque produced by an external magnetic field on the levitating magnet, stronger angular confinements can however be reached. For soft ferromagnets, best confinements are obtained for elongated bodies thanks to shape anisotropy [6]. In the experiments, we form elongated rods as the one shown in Fig.2-c) by levitating simultaneously a few particles in the trap and applying a magnetic field to bind them together using the attractive magnetic forces (See SI, section I). Once a rod is formed, we apply a homogeneous magnetic field  $B$ , of up to 0.1 T, using permanent magnets. For a soft oblate ferromagnet, the librational motion has a confinement frequency  $\omega_\phi = B\sqrt{V|n_r - n_a|/I_\phi\mu_0 n_a n_r}$  where  $V$

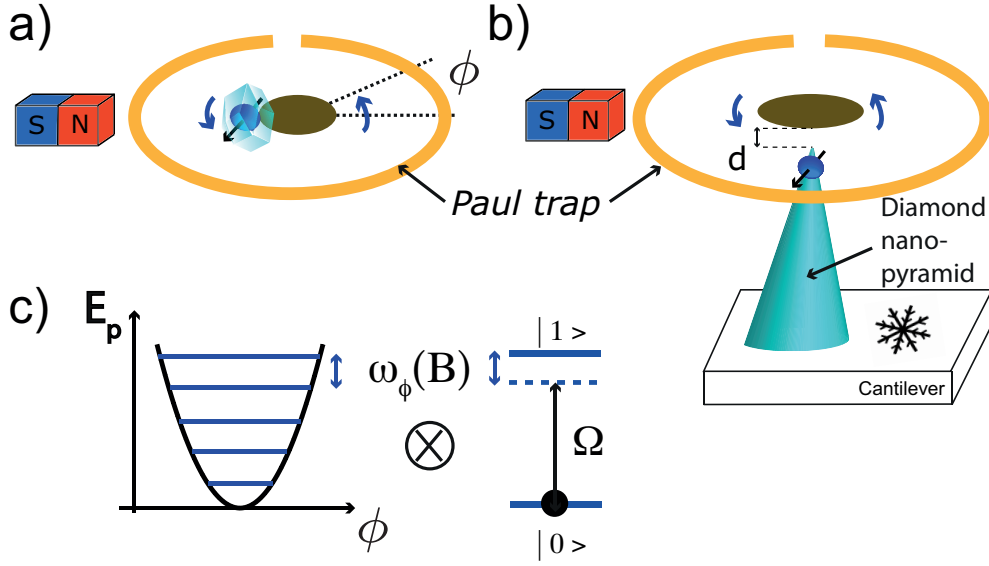


FIG. 1. Schematics showing two proposed platforms for strong spin-mechanical coupling using the librational motion of ferromagnets levitating in a Paul trap. In the first setup (a), a diamond is attached to a nano-magnet and coupled to the libration *via* the external static  $B$  field. In the second proposed setup (b), a nano-magnet is levitating at a distance  $d$  from the electronic spin of an NV center within a bulk diamond at cryogenic temperature. c) Potential energy of the magnetic field dependent harmonic libration resonantly coupled to the two-level spin system via a detuned microwave.

is the volume of the particle, and  $n_r, n_a$  are geometrical factors (See SI, section I and [6]).

We measure  $\omega_\phi$  using external coils that excite the librational mode of motion that we detect optically (see Fig.5-d) and SI). We show in Fig.5-e) a typical averaged time trace of our optical signal under a small magnetic field of 10 mT. As expected, the librational confinement is found at a much higher frequency ( $2\pi \times 20.7$  kHz) than the maximum confinement provided by the Paul trap (given by the trap frequency  $2\pi \times 2.5$  kHz). In addition to this large confinement frequency, a moderate vacuum of 1 mbar already enables the quality factor Q-factor to  $1.3 \times 10^3$  (see Fig.5-f)), which can be even larger under higher vacuum. We could finally verify the linear dependence of  $\omega_\phi$  with the strength of the external magnetic field  $B$ . As shown in Fig.5-g), at the highest field of 0.1 T, we find  $\omega_\phi = 2\pi \times (170 \pm 10)$  kHz in good agreement with the theory (see SI, section I). Calculations also show that a  $75 \times 25$  nm ellipsoidal soft ferromagnet would have a librational frequency of  $2\pi \times 24$  MHz under 0.1 T. One could even reach frequencies falling in the GHz range, by levitating permanent nano-magnets. These frequencies approach the relaxation rate of domain walls as given by the Landau-Lifshitz-Gilbert relaxation [53], offering prospects for investigating the rich interaction between phonons and spin angular momentum [54].

The present results show that magnetically confined ferromagnets levitating in a Paul trap form high quality mechanical oscillators. The measured Q-factor is, to our knowledge, the best reported value at this pressures for a levitating particle [47, 55], which might find applications in the field of ultra sensitive gyroscope [56] and torque

balances [57, 58]. Compared to other levitation systems, it also has the advantage to be free of the photon shot noise that ultimately limits the quality factor for optical trapped particles [59]. Another perspective is the study of the interplay between magnetism and orbital angular momentum, i.e. the Einstein-de Haas/Barnett effects. This platform can be used to test theoretical predictions that a non-rotating nano-magnet could be trapped in a static magnetic field [60]. Most importantly, this measured value of  $\omega_\phi/2\pi$  is very promising with regards to coupling the ferromagnet motion to NV centers' spin. It indeed largely exceeds the kHz linewidth of spin transition in isotopically purified bulk diamond [22], opening the way towards the two spin-mechanical schemes depicted in Fig. 1-a) and b) and that we now present in more detail.

*Coupling the magnet to NV centers.* NV centers combine both long lifetime and room temperature read-out of their electronic spins. They also have a natural quantization axis, which is essential for applying spin-dependent torques to distant particles or to levitating diamonds. One option for coupling the ferromagnet librational motion to the NV center is to directly attach diamonds to the ferromagnet. In this scheme (depicted in Fig. 1-a)), the projection of the external magnetic field onto the NV center quantization axis is changing as the hybrid particle rotates about its equilibrium position. The spin energy levels can thus change and a spin-dependent torque can be applied by the NV center onto the whole particle. Assuming that the magnetic field generated by the magnet is negligible, which can be the case for some positions of the ND on the magnet (measurements of the

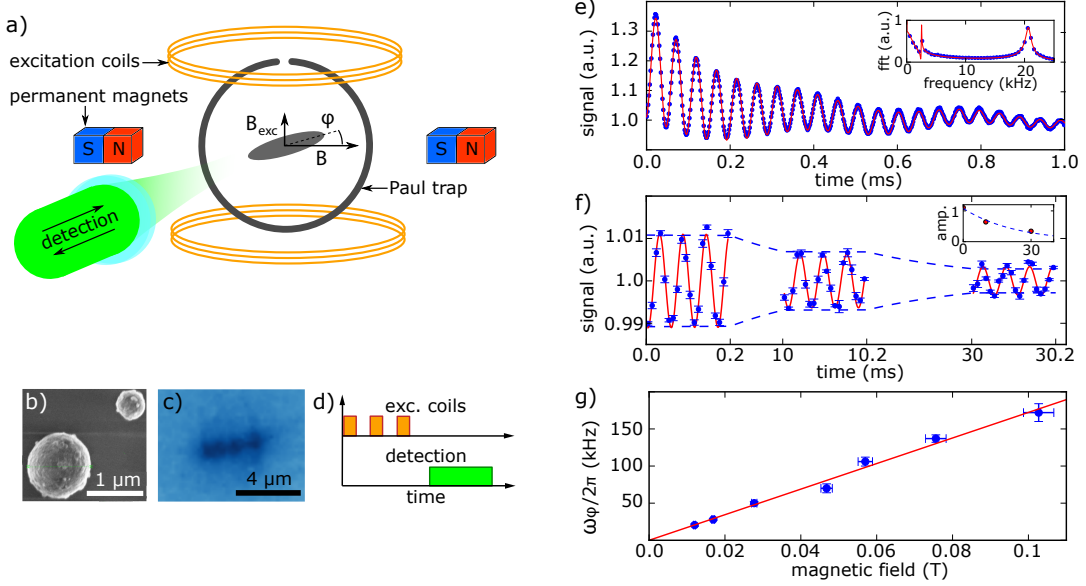


FIG. 2. a) Experimental setup. A ferromagnetic rod is levitating in a ring Paul trap. A pair of permanent magnets generates a uniform magnetic field  $\vec{B}$  that confines the particle orientation. Magnetic coils are used to excite the particle librational motion *via* a transverse field  $\vec{B}_{\text{exc}}$ . A laser is focussed on the particle to detect its motion. b) Scanning electron microscopy of the levitating iron particles. c) Image of a levitating ferromagnetic rod. d) Experimental sequence used for excitation and ring-down measurements. e) Magnet ring down measurement under atmospheric pressure. Points are experimental data. The solid line is a fit (explanations in the text). The inset shows the Fourier transform of the temporal signals. f) Ring down at a pressure of 1 mbar, measured at times 0, 10 and 30ms after excitation. The solid line is a fit. The inset shows the decaying amplitude of the oscillations. g) librational frequency  $\omega_\phi/2\pi$  versus magnetic field  $B$  for the magnetic rod shown in Fig.1-c).

magnetic field generated by the magnet on its surface are presented in the SI), the interaction Hamiltonian describing the spin-mechanical (SM) interaction is given by  $\hat{H}_{\text{int}} = \tilde{\lambda}_\phi \hat{S}_x (\hat{a}^\dagger + \hat{a})$ . Here,  $\hat{a}^\dagger$  and  $\hat{a}$  are the creation and annihilation operators of the phonon of the librational motion and  $\tilde{\lambda}_\phi$  is the SM coupling constant [9, 11]. A major difference between this scheme and the work of [9, 11], is that the magnet librational frequency  $\omega_\phi$  is now controlled by the external B-field amplitude. If we consider a composite system made of a spherical diamond and hard magnets with diameters of 40 nm and 20 nm respectively (see section II of the SI for details) a moderate homogeneous magnetic field of 30mT is enough to obtain a large confinement frequency  $\omega_\phi = 2\pi \times 3$  MHz and  $\tilde{\lambda}_\phi = 150$  kHz. Using isotopically enriched diamonds, the strong coupling condition would be attained without the need for high AC voltages and surface charge control.

Experimentally, we present first steps towards coupling the librational mode of hybrid levitating structures to the electronic spin. In one experiment, we prepare particles consisting of 100nm fluorescent nano-diamonds (NDs) containing many NV centers attached to the micron-sized iron particles (an SEM image is shown in Fig. 3-a)-i), and details of the fabrication are explained in the SI, section II). In another experiment, we evaporate a thin nickel layer on top of micron-sized diamond particles containing NV centers, which produces the particle depicted

in Fig. 3-a)-ii). Although the confinement frequency of both hybrid structures is not as high as with the ferromagnet rods, they can levitate stably with a librational frequency above the Paul trap librational confinement. As shown in Fig. 3 and in the section II of the SI, we could observe Electron-Spin-Resonances (ESR), spin-echos (b) and Rabi oscillations (c) from the NV centers in the first structure (i), similar to what has been observed recently with levitating micro-diamonds [3]. Operating under vacuum also revealed that laser heating was not as strong as what was observed in [2] with diamonds (see section II of the SI), due in part to the reflective property of the magnet. Iron indeed reflects most of the light, unlike particles that contain many impurities that couple to the phonons of the crystal after light absorption. Several technical issues were however encountered with this structure, and are listed in the SI. Let us turn to the second hybrid structure (ii). Using this structure, we could not only achieve coherent spin control, but the electronic spin sensitivity to magnetic fields could be exploited to detect the librational motion. To do this, parametric excitation of the motion was carried out similarly to in Fig. 3. Fig. 3-d)-i) shows ring down measurements obtained by measuring the change in the photoluminescence (PL) rate as the diamond oscillates. Using alternating blue and red microwave excitations of the spin, we could then extract the librational motion using the modulation of

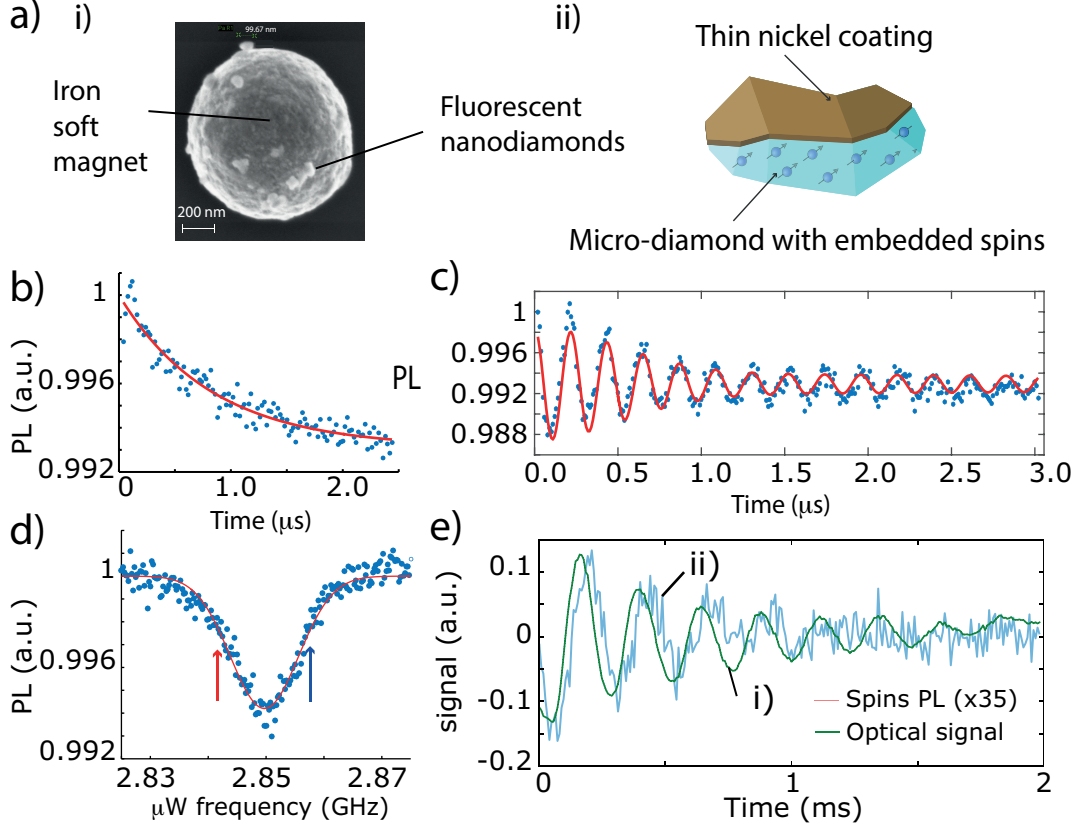


FIG. 3. a) i) Scanning electron microscope image of a hybrid particle composed of Fluorescent Nano-Diamonds (FND) on top of an iron ferromagnet. ii) Sketch of a hybrid diamond with a nickel coating b) Hahn-echo measurement ( $T_{2,echo}=825$  ns) and c) Rabi oscillations for an NV spin transition of the levitating hybrid particle depicted in a-i). d) ESR spectrum obtained from the hybrid particle ii). e) librational mode read-out from the PL change (i) and from the spin resonance shift (ii) at microwave frequencies showed by the arrows in (d).

the NV spins energy (Fig. 3-d-ii)). Interestingly, the evolution of the angle is slightly phase-shifted with respect to trace i), due to the interplay between the laser polarisation dynamics of the spins and the librational motion (see SI, section III).

Overall, the above results show promising steps towards the scheme (a) of Fig.1 for spin-mechanical coupling. In this scheme, the NV spin properties in pure bulk diamond at cryogenic temperatures can however not be fully exploited. We now turn to the second proposal for coupling the librational mode of a levitating magnet to a distant NV center in a nano-pyramid at 4K. Here, isotopically enriched diamonds could be used so that ESR lines much below the MHz can be obtained and high fidelity spin initialization is possible at such low temperatures [61]. The physics governing the SM interaction is here similar to in MRFM, but in the regime where dynamical back-action from long-lived spins can yield strong cooling and spin-motional coupling at the quantum level. Importantly, using the librational mode also enables modest magnetic field amplitudes for confining the considered mechanical oscillator mode.

Let us show how strong coupling to a distant NV can

be obtained with a levitating ferromagnet. We consider a hard ferromagnetic sphere levitating in the Paul trap in the presence of a fixed magnetic field and coupled to a single NV at a distance  $d$  from the magnet, as depicted in Fig. 4-a). The ferromagnet has a magnetic moment  $\vec{M}$  and librational mode frequency  $\omega_\phi$  determined by an external uniform external magnetic field  $\vec{B}_0$ . We study small rotations of the magnet about a single axis and we note  $\phi$  the angle between the particle and its equilibrium position. The coupling is obtained through the field  $\vec{B}_m$  generated by the micro-magnet at the NV position. This field depends on the angle  $\phi$  between the moment of the micro-magnet  $\vec{M}$  and its equilibrium position along the external magnetic field  $\vec{B}_0$  which can give rise to the coupling. To obtain a large spin-motion coupling, the NV center must be placed in close vicinity to the magnet ( $d < 1\mu m$ ) and the NV center axis must be aligned to the total magnetic field  $\vec{B}_t = \vec{B}_0 + \vec{B}_m$  to avoid spin state mixing by the transverse magnetic field (see SI, section IV). To enhance the SM coupling, the first order variation of  $\vec{B}_m$  in  $\phi$  should be maximal and along the NV axis. We find (see section IV of the



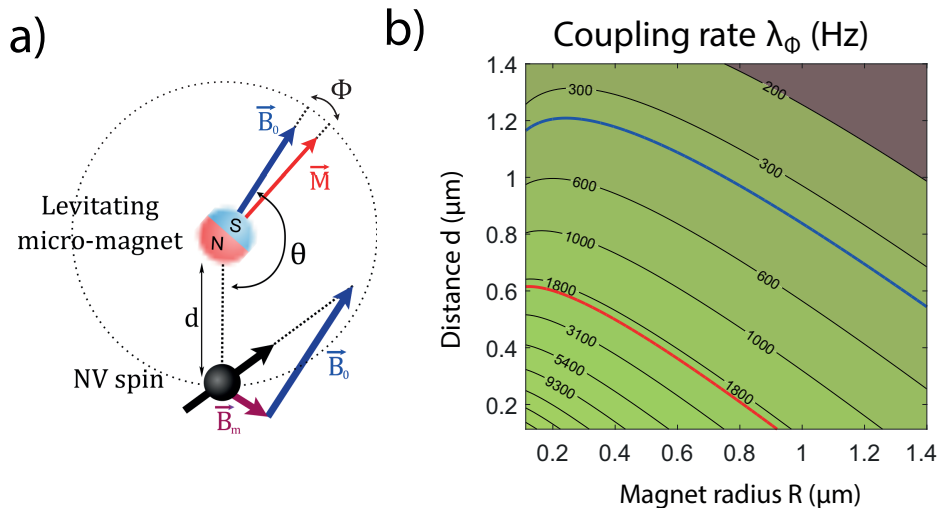


FIG. 4. a) NV center spin angle relative to the levitating magnet. The only degrees of freedom is  $\theta$  as the magnet is on average aligned to the magnetic field ( $\phi = 0$ ) and the NV center orientation is set along the total field  $\vec{B}_T$ . b) Coupling rate as a function of particle size and distance to the NV spin. The red (blue) curve correspond to  $\lambda_\phi = 1/T_2^*$  (370 Hz).

SI) that for a particular angle  $\theta_{op}$  the contribution along the NV axis is maximal and the one perpendicular to it cancels. However, using a diamond at 4 K lets us envision heralding protocols [24, 63] which employ the NV center high fidelity projective read-out [61] to counteract dephasing that occurs at a rate  $1/T_2^*$ . Here we illustrate such protocol in the simple case of one phonon Fock state preparation. First, the oscillator is cooled to the ground state through sideband cooling [9] using the zero-phonon line for spin initialization [61]. At a low enough pressure, heating from gas molecules will be negligible compared to cooling (see section IV of the SI for a detailed discussion) so the mean final phonon number will be solely limited by the high fidelity spin initialization (0.998 [61]). From there, a weak SM coupling generates superposition of spin-phonon entangled states and a following read-out of the spin will project it unto a Fock state corresponding to the measured spin state. If the spin-phonon exchange fails, both the spin and the oscillator can be reinitialized to minimize error at the expense of time. A coupling rate  $\lambda_\phi = 370$  Hz with a  $1\mu\text{m}$  magnet radius will yield a heralded state with a fidelity of 0.991 at a distance  $d = 1\mu\text{m}$ , which is now experimentally feasible.

In conclusion, we propose a method for coupling the librational mode of magnets levitating in a Paul trap to NV centers. Towards this aim, we successfully levitate magnets in a Paul trap and demonstrate large librational frequencies and Q-factors, which in itself offers the

possibility to connect orbital momentum and the spin degree of freedom [60] and to implement ultra-sensitive torque magnetometry [65]. Importantly, it leverages the technical bound on the maximum librational mode frequency that can be reached using a Paul trap angular potential only. We show that it then exceeds the spin transition linewidth of NV centers in distant CVD grown bulk diamonds, meaning that sideband cooling and motional state preparation are within reach. Last, we demonstrate coherent spin control of NV centers together with the read-out of the mechanical motion using NV centers' spins in hybrid ferromagnet-diamond particles which offers the prospects for realizing single-ion-like protocols such as coupling distant spins to the motional mode of the magnet [64].

## ACKNOWLEDGMENTS

We would like to thank José Palomo, Nabil Garoum and André Thiaville for technical assistance and fruitful discussions. GH acknowledges funding by the French National Research Agency (ANR) through the project SME-QUI and by the T-ERC program through the project QUOVADIS.

- 
- [1] D. Leibfried, R. Blatt, C. Monroe, and D. Wineland, *Rev. Mod. Phys.* **75**, 281 (2003).
  - [2] M. Kasevich and S. Chu, *Phys. Rev. Lett.* **67**, 181 (1991).

- [3] C. Monroe, D. M. Meekhof, B. E. King, and D. J. Wineland, **272**, 1131 (1996).
- [4] C. J. Myatt, B. E. M. King, Q. A. Turchette, C. A. Sackett, D. Kielpinski, W. M. Itano, C. A. Monroe, and D. J.

- Wineland, *Nature* **403**, 269 (2000).
- [5] P. Treutlein, D. Hunger, S. Camerer, T. W. Hänsch, and J. Reichel, *Phys. Rev. Lett.* **99**, 140403 (2007).
- [6] N. Lambert, I. Mahboob, M. Pioro-Ladrière, Y. Tokura, S. Tarucha, and H. Yamaguchi, *Phys. Rev. Lett.* **100**, 136802 (2008).
- [13] P. Rabl, P. Cappellaro, M. V. G. Dutt, L. Jiang, J. R. Maze, and M. D. Lukin, *Phys. Rev. B* **79**, 041302 (2009).
- [8] M. Scala, M. S. Kim, G. W. Morley, P. F. Barker, and S. Bose, *Phys. Rev. Lett.* **111**, 180403 (2013).
- [9] C. Wan, M. Scala, G. W. Morley, A. A. Rahman, H. Ulbricht, J. Bateman, P. F. Barker, S. Bose, and M. S. Kim, *Phys. Rev. Lett.* **117**, 143003 (2016).
- [10] J.-Q. Zhang, S. Zhang, J.-H. Zou, L. Chen, W. Yang, Y. Li, and M. Feng, *Optics Express* **21**, 29695 (2013), arXiv:1307.3952 [quant-ph].
- [11] Y. Ma, Z.-q. Yin, P. Huang, W. L. Yang, and J. Du, *Phys. Rev. A* **94**, 053836 (2016), arXiv:1603.05807 [quant-ph].
- [12] Z. Yin, N. Zhao, and T. Li, *Science China Physics, Mechanics & Astronomy* **58**, 1 (2015).
- [13] P.-B. Li, Z.-L. Xiang, P. Rabl, and F. Nori, *Phys. Rev. Lett.* **117**, 015502 (2016).
- [14] M. Abdi, M.-J. Hwang, M. Aghtar, and M. B. Plenio, *Phys. Rev. Lett.* **119**, 233602 (2017).
- [9] T. Delord, L. Nicolas, Y. Chassagneux, and G. Hétet, *Phys. Rev. A* **96**, 063810 (2017).
- [16] E. R. MacQuarrie, M. Otten, S. K. Gray, and G. D. Fuchs, *Nature Communications* **8**, 14358 (2017), arXiv:1605.07131 [quant-ph].
- [17] A. Bassi, K. Lochan, S. Satin, T. Singh, and H. Ulbricht, *Rev Mod Phys* **85** (2013), 10.1103/RevModPhys.85.471.
- [18] A. Gruber, A. Drabenstedt, C. Tietz, L. Fleury, J. Wrachtrup, and C. v. Borczyskowski, *Science* **276**, 2012 (1997).
- [21] G. Balasubramanian, P. Neumann, D. Twitchen, M. Markham, R. Kolesov, N. Mizuochi, J. Isoya, J. Achard, J. Beck, J. Tessler, *et al.*, *Nature materials* **8**, 383 (2009).
- [22] P. C. Maurer, G. Kucsko, C. Latta, L. Jiang, N. Y. Yao, S. D. Bennett, F. Pastawski, D. Hunger, N. Chisholm, M. Markham, D. J. Twitchen, J. I. Cirac, and M. D. Lukin, **336**, 1283 (2012).
- [21] N. Bar-Gill, L. M. Pham, A. Jarmola, D. Budker, and R. L. Walsworth, *Nature Communications* **4**, 1743 EP (2013).
- [22] P. Rabl, S. J. Kolkowitz, F. H. L. Koppens, J. G. E. Harris, P. Zoller, and M. D. Lukin, *Nature Physics* **6**, 602 (2010).
- [23] P. Rabl, *Phys. Rev. B* **82**, 165320 (2010).
- [24] S. D. Bennett, S. Kolkowitz, Q. P. Unterreithmeier, P. Rabl, A. C. B. Jayich, J. G. E. Harris, and M. D. Lukin, *New Journal of Physics* **14**, 125004 (2012).
- [25] K. V. Keesidis, S. D. Bennett, S. Portolan, M. D. Lukin, and P. Rabl, *Phys. Rev. B* **88**, 064105 (2013).
- [26] O. Arcizet, V. Jacques, A. Siria, P. Poncharal, P. Vincent, and S. Seidelin, *Nat Phys* **7**, 879 (2011).
- [27] S. Kolkowitz, A. C. Bleszynski Jayich, Q. P. Unterreithmeier, S. D. Bennett, P. Rabl, J. G. E. Harris, and M. D. Lukin, *Science* **335**, 1603 (2012).
- [28] E. R. MacQuarrie, T. A. Gosavi, N. R. Jungwirth, S. A. Bhavé, and G. D. Fuchs, *Phys. Rev. Lett.* **111**, 227602 (2013).
- [29] J. Teissier, A. Barfuss, P. Appel, E. Neu, and P. Maletinsky, *Physical Review Letters* **113**, 020503 (2014), arXiv:1403.3405 [cond-mat.mes-hall].
- [30] P. Ovartchaiyapong, K. W. Lee, B. A. Myers, and A. C. B. Jayich, *Nature Communications* **5**, 4429 EP (2014), article.
- [31] E. R. MacQuarrie, T. A. Gosavi, A. M. Moehle, N. R. Jungwirth, S. A. Bhavé, and G. D. Fuchs, *Optica* **2**, 233 (2015).
- [32] A. Barfuss, J. Teissier, E. Neu, A. Nunnenkamp, and P. Maletinsky, *Nature Physics* **11**, 820 EP (2015).
- [33] D. A. Golter, T. Oo, M. Amezcu, K. A. Stewart, and H. Wang, *Physical Review Letters* **116**, 143602 (2016), arXiv:1603.03804 [quant-ph].
- [34] Z.-q. Yin, T. Li, X. Zhang, and L. M. Duan, *Phys. Rev. A* **88**, 033614 (2013).
- [35] D. E. Chang, C. A. Regal, S. B. Papp, D. J. Wilson, J. Ye, O. Painter, H. J. Kimble, and P. Zoller, *Proceedings of the National Academy of Sciences* **107**, 1005 (2010).
- [36] O. Romero-Isart, A. C. Pflanzer, M. L. Juan, R. Quidant, N. Kiesel, M. Aspelmeyer, and J. I. Cirac, *Phys. Rev. A* **83**, 013803 (2011).
- [11] Y. Ma, T. M. Hoang, M. Gong, T. Li, and Z.-q. Yin, *Phys. Rev. A* **96**, 023827 (2017).
- [38] L. P. Neukirch, J. Gieseler, R. Quidant, L. Novotny, and A. Nick Vamivakas, *Optics Letters* **38**, 2976 (2013).
- [39] T. M. Hoang, J. Ahn, J. Bang, and T. Li, *Nature Communications* **7**, 12250 EP (2016).
- [40] T. M. Hoang, Y. Ma, J. Ahn, J. Bang, F. Robicheaux, Z.-Q. Yin, and T. Li, *Phys. Rev. Lett.* **117**, 123604 (2016).
- [41] S. Kuhn, A. Kosloff, B. A. Stickler, F. Patolsky, K. Hornberger, M. Arndt, and J. Millen, *Optica* **4**, 356 (2017).
- [42] A. T. M. A. Rahman, A. C. Frangskou, M. S. Kim, S. Bose, G. W. Morley, and P. F. Barker, *Scientific Reports* **6**, 21633 EP (2016).
- [43] A. Kuhlicke, A. W. Schell, J. Zoll, and O. Benson, *Applied Physics Letters* **105** (2014).
- [1] T. Delord, L. Nicolas, L. Schwab, and G. Hétet, *New Journal of Physics* **19**, 033031 (2017).
- [2] T. Delord, L. Nicolas, M. Bodini, and G. Hétet, *Applied Physics Letters* **111**, 013101 (2017).
- [3] T. Delord, P. Huillery, L. Schwab, L. Nicolas, L. Lecordier, and G. Hétet, *Phys. Rev. Lett.* **121**, 053602 (2018).
- [47] G. P. Conangla, A. W. Schell, R. A. Rica, and R. Quidant, *Nano Letters* (2018).
- [48] J.-F. Hsu, P. Ji, C. W. Lewandowski, and B. D'Urso, *Scientific Reports* **6**, 30125 EP (2016).
- [49] C. L. Degen, M. Poggio, H. J. Mamin, C. T. Rettner, and D. Rugar, *Proceedings of the National Academy of Sciences* **106**, 1313 (2009), <https://www.pnas.org/content/106/5/1313.full.pdf>.
- [50] D. Rugar, R. Budakian, H. J. Mamin, and B. W. Chui, *Nature* **430**, 329 EP (2004).
- [51] L. Rondin, J.-P. Tetienne, T. Hingant, J.-F. Roch, P. Maletinsky, and V. Jacques, *Reports on Progress in Physics* **77**, 056503 (2014).
- [6] J. J. Abbott, O. Ergeneman, M. P. Kummer, A. M. Hirt, and B. J. Nelson, *IEEE Transactions on Robotics* **23**, 1247 (2007).
- [53] K. Gilmore, Y. U. Idzerda, and M. D. Stiles, *Phys. Rev. Lett.* **99**, 027204 (2007).
- [54] Y. Tserkovnyak, A. Brataas, G. E. W. Bauer, and B. I. Halperin, *Rev. Mod. Phys.* **77**, 1375 (2005).

- [55] T. M. Hoang, Y. Ma, J. Ahn, J. Bang, F. Robicheaux, Z.-Q. Yin, and T. Li, Phys. Rev. Lett. **117**, 123604 (2016).
- [56] C. Shearwood, K. Y. Ho, C. B. Williams, and H. Gong, Sensors and Actuators A: Physical **83**, 85 (2000).
- [57] M. Wu, A. C. Hryciw, C. Healey, D. P. Lake, H. Jayakumar, M. R. Freeman, J. P. Davis, and P. E. Barclay, Phys. Rev. X **4**, 021052 (2014).
- [58] P. H. Kim, B. D. Hauer, C. Doolin, F. Souris, and J. P. Davis, Nature Communications **7**, 13165 EP (2016), article.
- [59] V. Jain, J. Gieseler, C. Moritz, C. Dellago, R. Quidant, and L. Novotny, Physical review letters **116**, 243601 (2016).
- [60] C. C. Rusconi, V. Pöschhacker, K. Kustura, J. I. Cirac, and O. Romero-Isart, Phys. Rev. Lett. **119**, 167202 (2017), arXiv:1703.09346 [quant-ph].
- [61] L. Robledo, L. Childress, H. Bernien, B. Hensen, P. F. Alkemade, and R. Hanson, Nature **477**, 574 (2011).
- [62] M. Brownnutt, M. Kumph, P. Rabl, and R. Blatt, Rev. Mod. Phys. **87**, 1419 (2015).
- [63] D. B. Rao, S. A. Momenzadeh, and J. Wrachtrup, Physical review letters **117**, 077203 (2016).
- [64] X.-Y. Chen and Z.-q. Yin, Phys. Rev. A **99**, 022319 (2019).
- [65] P. H. Kim, B. D. Hauer, C. Doolin, F. Souris, and J. P. Davis, Nature Communications **7**, 13165 EP (2016).

## SUPPLEMENTARY MATERIAL

### I. LEVITATION OF FERROMAGNETIC PARTICLES IN PAUL TRAPS

Ferromagnetic particles are trapped using the same setup than for the trapping of diamonds, described in details in [1–3]. The experimental set-up is depicted in Fig.1. The trap and the objective are enclosed in a vacuum chamber. The trap is a ring Paul-Straubel trap [4, 5]. It consists in a small 25  $\mu\text{m}$  thick tungsten wire with an inner radius of 200  $\mu\text{m}$ . It is oriented so that the ring plane is perpendicular to the optical axis.

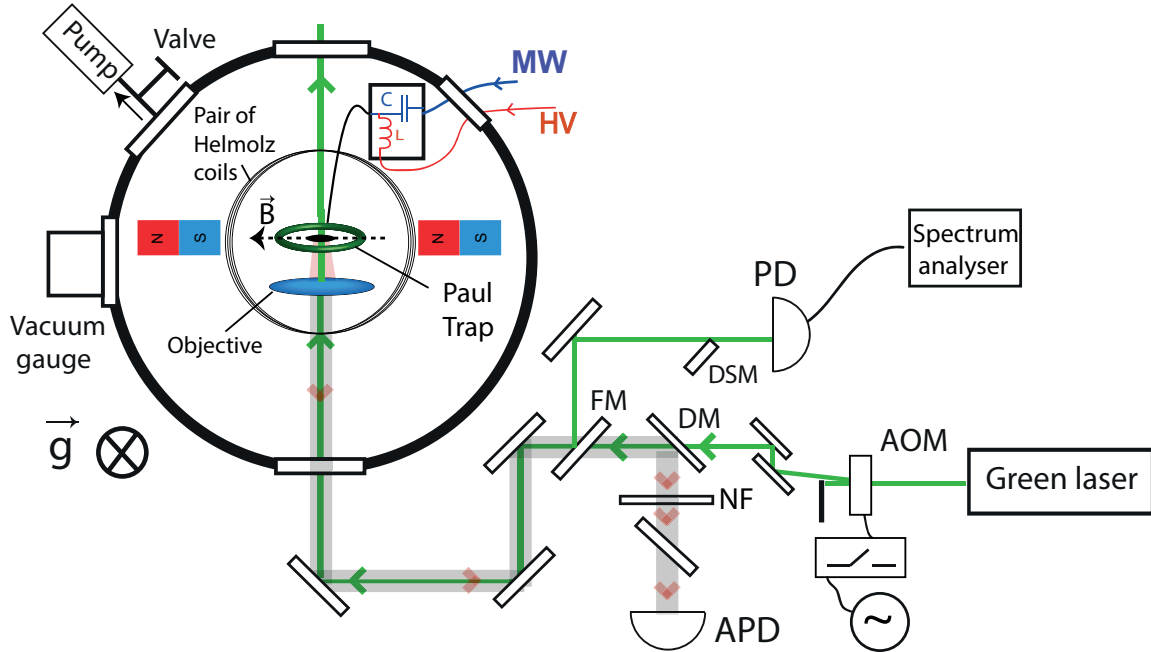


FIG. 5. Schematics of the experimental apparatus. The Paul trap, objective, and Bias Tee are enclosed in a vacuum chamber. A green laser is focused onto particles levitating in the Paul trap. Light reflected from the levitating particle is collected by the same objective and measured either on an avalanche photodiode (APD) or on a spectrometer. DM= dichroic mirror, NF=Notch filter centered at 532 nm. FM=flipping mirror. PD=Photodetector, HV=High Voltage, MW= Microwave. DSM=D-shaped mirror. AOM= Acousto-Optic-Modulator

The particles that we mostly used are 98% pure iron particles that are spherical in shape (Goodfellow, ref. FE006045). While their diameters is rated to be from 1 to 6  $\mu\text{m}$ , scanning electron microscopy images of our

sample shows that diameters vary roughly from 0.5 to 3  $\mu\text{m}$  with most of the particles having a diameter around 1  $\mu\text{m}$  (see Fig.2). The particles come in the form of a dry powder and did not undergo specific surface processing. They are injected using a small metallic tip that is dipped into the powder and brought in the vicinity of the trap. With such micron-sized particles, we can operate the trap with a peak-to-peak voltage ranging from  $V_{ac}=100$  V to 4000 V at driving frequencies in the kHz range. Particles are generally injected under ambient conditions at  $V_{ac}=4000$  V and at a trap frequency of a few kHz.

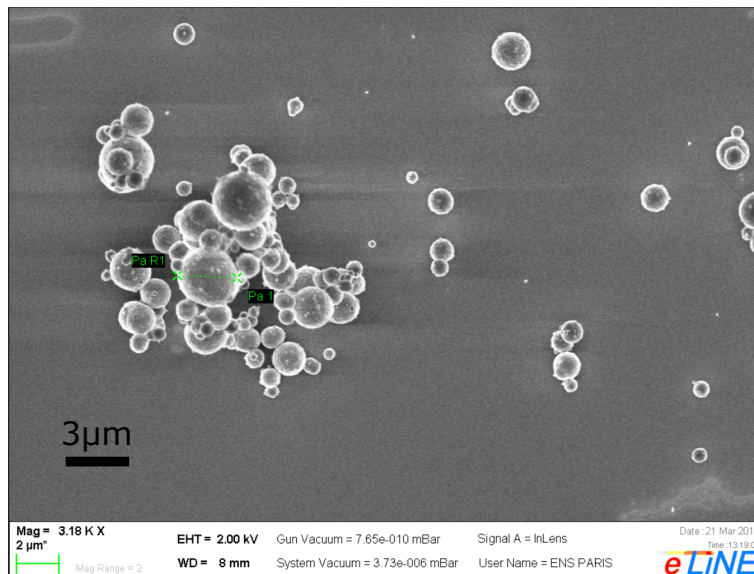


FIG. 6. Scanning Electron Microscopy (SEM) image of a few iron particles deposited on a coverslip

Overall, the injection technique and trapping operations are essentially the same than for micro-diamonds. However, while levitating diamonds are always negatively charged, we found that both positively and negatively charged iron particles can be stably levitating in the trap. This indicates that the tribo-electricity, responsible for the charge acquired by the particles during injection, differs between iron and diamond. Given these observations, on one levitating iron particle, both positive and negative charge patches may be present simultaneously. This is an important observation with regards to the assembly operation that we describe next.

#### A. *In-situ* assembling of ferromagnetic particles

To benefit from the potentially large librational frequencies of the ferromagnetic particles offered by shape anisotropy, we form elongated rods by assembling few spherical iron particles. This is done *in-situ*, *i.e.* within the Paul trap, using the following procedure:

- 1- We inject several iron particles simultaneously in the Paul trap. Given the large size of the trap (200  $\mu\text{m}$  diameter) compared to the size of the particles, tens of particles can be levitated simultaneously.
- 2- We lower the trap potential and eject some particles using air currents in order to then bind only 2 to 4 particles together (the optimum aspect ration for large librational frequencies is calculated next).
- 3- We increase the Paul trap confinement by reducing the trap frequency in order to bring the particles as close as possible from each other. At this stage, the particles still repeal each other due to electrostatic forces, forming a so-called Coulomb crystal.
- 4- We then apply a magnetic field by bringing manually a permanent magnet next to the trap. Magnetic forces acting between the different particles which are then magnetized, are attractive. For sufficiently high magnetic field, of the order of few tens of Gauss, attractive magnetic forces overcome the repulsive electrostatic ones and the particles bind together, forming a rod aligned in the direction of the magnetic field. The eventual presence of charge patches of different sign on the particles, mentioned in the previous section, might also assist the binding process.

Once a rod is formed, particles remain bonded together even when the external magnetic field is nulled, thanks to remanent magnetization and/or Van-der-Waals forces.

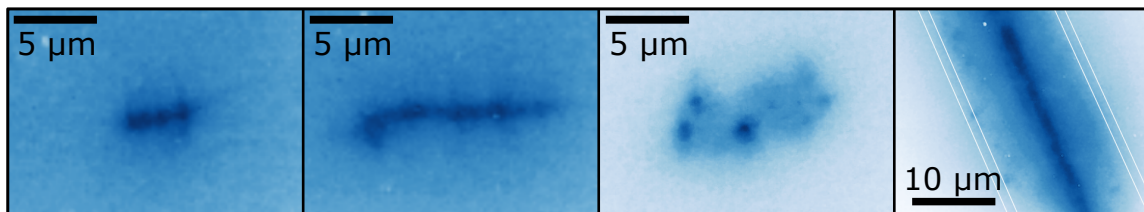


FIG. 7. Images of 3 levitating rods and of the 15  $\mu\text{m}$  diameter wire used to determine the magnification of the imaging system

As shown in Fig.3 we could image the levitating particles. For this we shine incoherent light onto the particles and use the objective to image the particles onto a CCD camera.

### B. Librational mode excitation and optical detection

In the experiments, we use a pair of external coils in Helmholtz configuration in order to excite the librational mode of the levitating ferromagnet. The coils generate a magnetic field perpendicular to the field produced by the permanent magnets used to confine the orientation of the particle, allowing us to displace the particle from its equilibrium orientation. We can thus excite the librational mode by switching the current flowing through the coils. We typically run the coils with a current of 0.5A that is switched off in around 2  $\mu\text{s}$  using a fast electronic switch (EDR83674/2 from company EDR). While the coils mainly excite the librational mode of motion, the center of mass motion is also weakly excited. To favor the excitation of the librational mode while minimizing the center of mass excitation, the coils current is switched ON and OFF, 3 times, at a frequency close to the librational frequency (See Fig.1d in the main text).

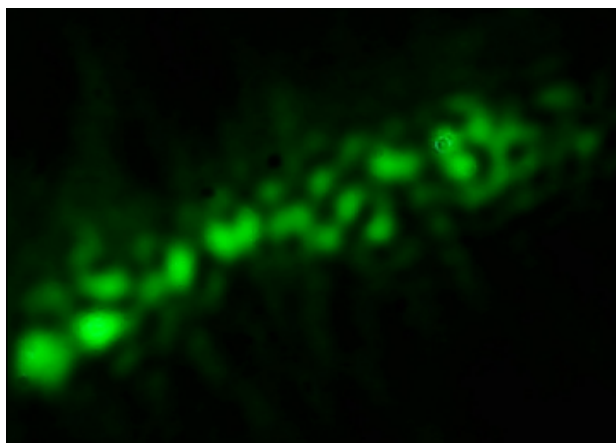


FIG. 8. Image of the particle speckle obtained at the levitating particle image plane under coherent illumination with green laser light.

After excitation, we look at the particle motion using optical detection. With the objective inside the vacuum chamber, we focused a green laser onto the particle and collect the reflected light. As shown in Fig.4, at the particle image plane which is located few tens of centimeters away, an image of the particle is formed with an additional speckle feature coming from the coherent nature of the illumination. To detect our signal (shown in Fig. 2 in the main text), we focus a small area of this image onto a single-mode optical fibre and detect the photons transmitted through the fibre with a single photon avalanche photodiode. Thanks to the speckle feature, the detected signal is highly sensitive on the particle position and orientation. For a given levitating particle, we can optimize, in real time, the signal coming from the angular displacement of the particle by selecting the most favorable region of the particle image. To do this, we look at our optical signal while switching the excitation coils at a frequency of 1 Hz.

Our detection method is not intrinsically linear, i.e. the optical signal is not necessarily linear with the angular displacement, and indeed, harmonics of the confinement frequencies can be seen on the signal. However, quasi linearity



can be obtained by finely adjusting the detection zone on the particle image. The data in Fig. 3-a) are well fitted by the sum of 3 exponentially damped sinusoids, indicating that our signal reproduces quite faithfully the particle motion. Quasi linearity is also seen in the spectrum of the time trace, shown in the inset of Fig. 3-a) where we have highlighted the barely visible 2nd order harmonic features.

### C. Magnetic confinement of ferromagnetic particles

We present here theoretical estimations of the torque applied to ferromagnetic particles by an external magnetic field and of the corresponding librational frequency.

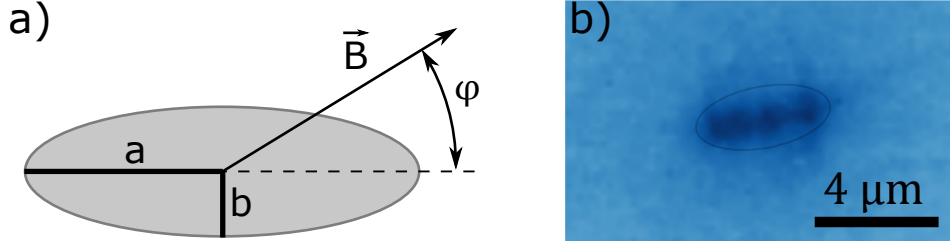


FIG. 9. a) Prolate ellipsoid. b) Image of the particle used for the measurement of the magnetic confinement frequency versus magnetic field shown in the main text. An ellipsoid with approximatively the same dimensions is drawn on top of the particle.

We consider first the torque resulting from shape anisotropy applied on a prolate ellipsoidal soft magnetic body, which tends to align the long axis of the particle along the magnetic field direction (see Fig.6a). In [6], a model to calculate magnetic forces and torques applied on ideal soft ferromagnetic axially symmetrical bodies has been developed and tested experimentally with excellent quantitative agreement. The torque formula presented below is taken from there. We consider a particle with axial and radial dimensions  $2a$  and  $2b$ . The torque applied on the body by a weak external magnetic field  $B$  is given by

$$T_{soft}(\phi) = \frac{V(n_r - n_a)}{2\mu_0 n_a n_r} B^2 \sin(2\phi) \quad (1)$$

where  $\phi$  is the angle between the magnetic field and the body symmetry axis,  $V = \frac{4\pi}{3}ab^2$  is the volume of the particle,  $\mu_0$  is the vacuum magnetic permeability and  $n_r, n_a \in [0, 1]$  are the so-called demagnetisation factors. Those are purely geometrical and can be calculated analytically for ellipsoidal bodies [7]

$$n_a = \frac{1}{R^2 - 1} \left( \frac{R}{2\sqrt{R^2 - 1}} \ln \left( \frac{R + \sqrt{R^2 - 1}}{R - \sqrt{R^2 - 1}} \right) - 1 \right)$$

$$n_r = \frac{1}{2}(1 - n_a)$$

where  $R = a/b$  is the aspect ratio of the particle. This expression of the torque is valid for a soft ferromagnetic material with large magnetic susceptibility ( $\chi \gg 1$ ) and a magnetic field such as

$$B < \mu_0 m_s \frac{n_a n_r \sqrt{2}}{\sqrt{n_a^2 + n_r^2}}$$

where  $m_s$  is the magnetisation at saturation of the material. It is quite remarkable that, under those conditions, the torque does not depend on the magnetic properties of the body but only on its geometry.

From kinematics principles, we find that the confinement frequency for the angle  $\phi$  resulting from the magnetic torque  $T_{soft}$  is given by

$$\omega_\phi = \sqrt{\frac{V(n_r - n_a)}{I_\phi \mu_0 n_a n_r}} B \quad (2)$$

where  $I_\phi = \rho V(a^2 + b^2)/5$  is the relevant component of the particle rotational inertia,  $\rho$  being the particle density.

The librational frequency is proportional to the applied magnetic field and, for a given aspect ratio, it is inversely proportional to the particle size. This latter property can be seen by writing

$$\frac{V}{I_\phi} = \frac{1}{V^{\frac{2}{3}}} \frac{5}{\rho} \left( \frac{4\pi}{3} \right)^{\frac{2}{3}} \frac{R^{\frac{2}{3}}}{R^2 + 1}$$

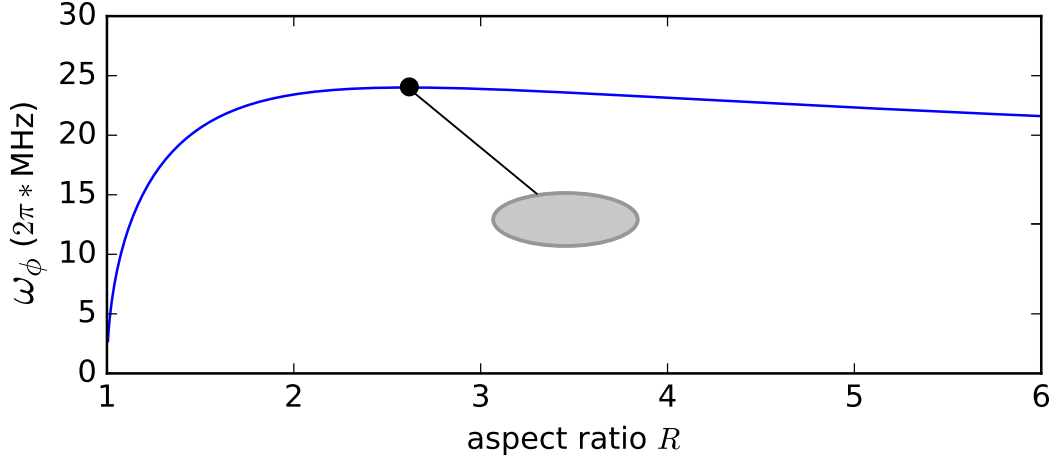


FIG. 10. Magnetic confinement frequency versus aspect ratio for a soft ferromagnetic ellipsoid with fixed minor-axis. The ellipse drawn in the middle of the figure has an aspect ratio of  $\approx 2.6$  which gives the highest magnetic confinement. The minor-axis is set to 25nm and the magnetic field to 0.1T.

In Fig.7, we plot  $\omega_\phi$  versus the particle aspect ratio for a fixed minor-axis size. Best confinement frequency is obtained for an aspect ratio of  $R \approx 2.606$ .

By approximating our experimentally trapped elongated rods with ellipsoids, we can compare our experimental measurement of  $\omega_\phi$  with theoretical calculations. In the experiment, with the particle shown in Fig.6b, we measured  $\omega_\phi \approx 2\pi \times 170\text{kHz}$  at a field of 0.1T. Theoretically, for an ellipsoid of  $5.4\mu\text{m} \times 2.5\mu\text{m}$  as drawn on top of the image, and taking an iron density of  $7.86\text{ g/cm}^3$ , we find  $\omega_\phi \approx 2\pi \times 240\text{kHz}$  at a field of 0.1T. This is in fair agreement with the experimental value given the rough approximation made on the particle shape. For this particle shape, the torque equation is valid for magnetic fields below 0.46T, assuming a magnetisation at saturation of iron of 2.2T. This confirms that a linear dependence of  $\omega_\phi$  with the magnetic field is effectively expected for the range of fields used in the experiments (from 0 to 0.1T). Since  $\omega_\phi$  increases with decreasing particle size, larger confinement frequencies could be obtained for levitating nano particles. We calculate that, for an ellipsoid of  $75\text{nm} \times 25\text{nm}$  under a field of 0.1T, we would obtain  $\omega_\phi \approx 2\pi \times 24\text{MHz}$ .

Hard ferromagnetic materials (permanent magnets) could offer much stronger magnetic confinements than their soft ferromagnetic counterparts. For a magnet with uniform magnetisation  $m$ , as long as the external field does not modify the magnetisation of the material, the torque which tends to align the particle magnetisation direction along the external magnetic field is simply given by

$$T_{\text{hard}}(\phi) = VmB \sin(\phi) \quad (3)$$

where  $\phi$  is now the angle between the magnetisation and magnetic field directions. This holds for any particle shape. Magnetic confinement frequencies are then given by  $\omega_\phi = \sqrt{VmB/I_\phi}$ . For a  $5.4\mu\text{m} \times 2.5\mu\text{m}$  ellipsoidal neodymium particle, under a field of 0.1T, we find  $\omega_\phi \approx 2\pi \times 18\text{MHz}$ . We assume for this a magnetisation of 1.6T and a density of  $7.4\text{ g/cm}^3$ . For a smaller  $75\text{nm} \times 25\text{nm}$  ellipsoid, we have  $\omega_\phi \approx 2\pi \times 1.3\text{GHz}$ . Experimentally, trapping micro or nano-particles of a hard ferromagnetic material would be highly beneficial to boost confinement frequencies. However, because of the strong attractive magnetic forces, it is difficult to isolate the particles from each other.

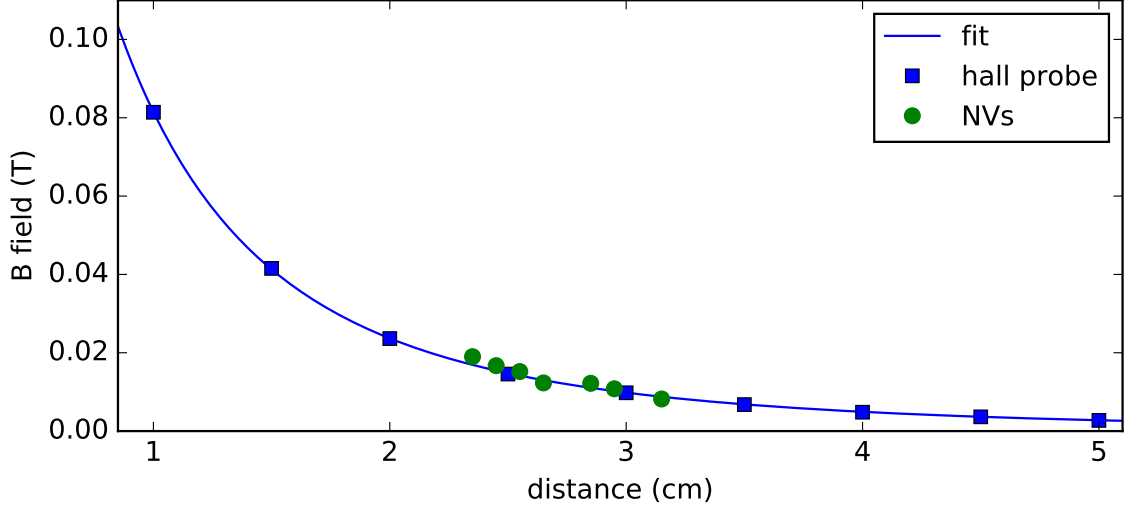


FIG. 11. Calibration of the magnetic field generated by the permanent magnets versus their distance  $d$  from the trap center. Both a Hall probe and NV centers contained in a micro-diamond has been used as magnetic sensors. The solid line is a  $1/d^3$  fit to the Hall probe data, used to evaluate the magnetic field in the experiments shown in Fig.1g) in the main text.

#### D. Magnetic field calibration

We calibrated the magnetic field generated by the two permanent magnets as a function of their distance from the levitated particle using a Hall probe. We show in Fig. 8 the data taken for this calibration. We could also double check the calibration using, as magnetic sensors, NV centers contained in a micro-diamond deposited directly on the ring trap. One can indeed infer the magnetic field seen by NV centers by performing Electronic Spin Resonances (ESR) scans on the NV centers spins [8]. For this, we calculate numerically the spin transitions energy of a NV center for all magnetic field strengths (up to 0.1T) and relative orientations with the NV axes. Experimental measurements of the spin transition frequencies is then compared with calculations to identify the magnetic field seen by the NV centers.

## II. NV CENTERS IN NANODIAMONDS ATTACHED TO LEVITATING FERROMAGNETIC PARTICLES

Obtaining librational frequencies larger than 1 kHz is a relatively straightforward task with levitating ferromagnets as opposed to levitating diamonds, where the librational mode frequency depends on dipole or quadrupolar distribution of charges on the diamond surface which are sample dependent. We thus propose a protocol that uses nanodiamonds attached to ferromagnets in order to increase the trapping frequency.

#### A. Preparation of the hybrid system

The employed nanodiamonds are bought in the form of a solution containing fluorescent nanodiamonds (brFND-100) from FND biotech, and contain a large fraction of NV centers ( $>1000$  NV centers per particle are quoted by the manufacturer). We show in Fig.10 a confocal map of many FNDs nebulized on a quartz coverslip. Single FND are clearly seen and spin characterisation could be performed on this sample.

As mentioned in the main text, we then attach these NDs to the ferromagnets. This was done using the following procedure:

- 1- Several iron particles are cast on a quartz coverslip.
- 2- A solution containing nanodiamonds (100 nm in diameter) with a large concentration of NV centers is prepared and injected in the reservoir of ultrasonic nebulizer and the solution is nebulized on top of the quartz coverslip



FIG. 12. SEM image of three iron particles with several nanodiamonds attached to it.

supporting the iron particles. A SEM image of the mixture is shown in figure 12 and an image showing a single iron particle is shown in the main text. Their concentration has been chosen so that single nanodiamonds could be excited optically once in the trap.

- 3- The prepared sample is then scrapped using a small metallic wire and brought close to the trap for injection and the PL rate, ESR, echo signals are monitored in the same way as demonstrated in [3].

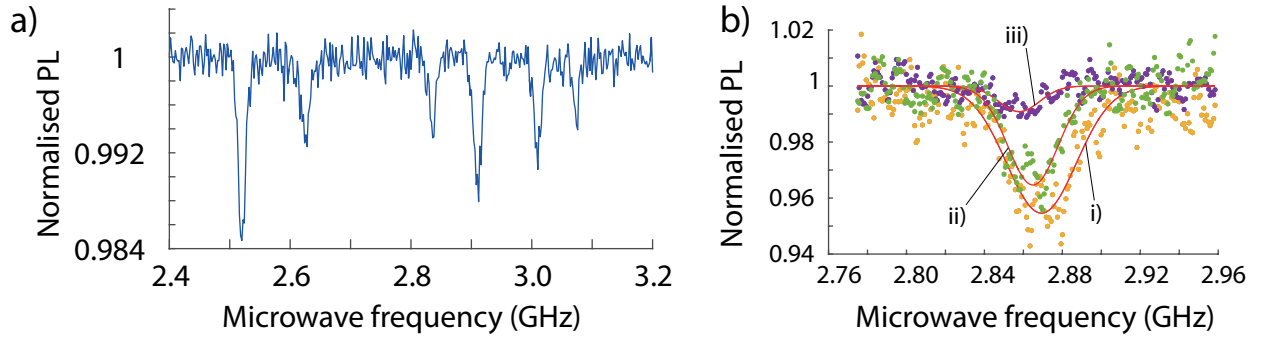


FIG. 13. a) ESR spectrum from NV centers in a nanodiamond attached to a levitating ferromagnet. b) ESR spectra taken without a magnetic field at three different vacuum pressures : 0.5, 0.07 and 0.01 mbar for traces i) ii) iii) respectively.

We encounter several issues with the characterization of the hybrid structure when observing the ESR. One subtle point is that, if some ESR lines overlap (which is a problem when one wishes to perform efficient Rabi oscillations), tuning the external magnetic field orientation with respect to the diamond axis is not enough to lift this degeneracy. The magnet main axis follows the B field angle so the NDs that are attached to it are also aligned in the very same way as the B field is rotated. If this situation occurs, another ND on the particle or another sample must be chosen. This effect does not impact the spin-mechanical coupling mechanism since the magnet inertia will let the NV feel a varying magnetic field.

Another problem that was encountered is that the ESR contrast, already in the absence of magnetic field, was often reduced compared to the optimum (10%) that is typically observed. Spin control was thus not possible for all levitating hybrid particles. The chemical properties of the hybrid particles or the presence of charges patches close to the nano-diamonds could be responsible for this, but further investigations would be needed to nail down this issue.

One promising feature however is that most hybrid particle are less sensitive to the laser torque. Less noisy ESR spectra can thus be obtained. Fig. 13-a) shows one such spectra, taken at room temperature, which displays similar properties (contrast and width) than ESRs typically observed with MSY micro-diamonds [3]. Further, the temperature of the assembly can be kept rather low even at significant vacuum levels even when laser light is shone to the particle. Fig. 13-b) shows ESRs taken at three different vacuum levels. The temperature of the particle can be estimated using a similar procedure than in [2], and we found a temperature of around 400 K for trace ii), which was obtained at under 0.07 mbars. Compared to the experiment performed in [2], at least an order of magnitude in pressure could thus be gained, when using similar green laser powers ( $100\mu\text{W}$ ). As mentioned in the main text, the reason is likely to be that iron reflects most of the impinging light instead of absorbing it. Here this could also be because the ND dissipates heat more efficiently than micro-diamonds due to the larger surface to mass ratio of the NDs compared to the micro-diamonds. The fast drop of the ESR contrast in trace iii) is unexpectedly large, which may also stem from chemical reactions or patch potentials in combination with the normal contrast drop due to the large temperature.

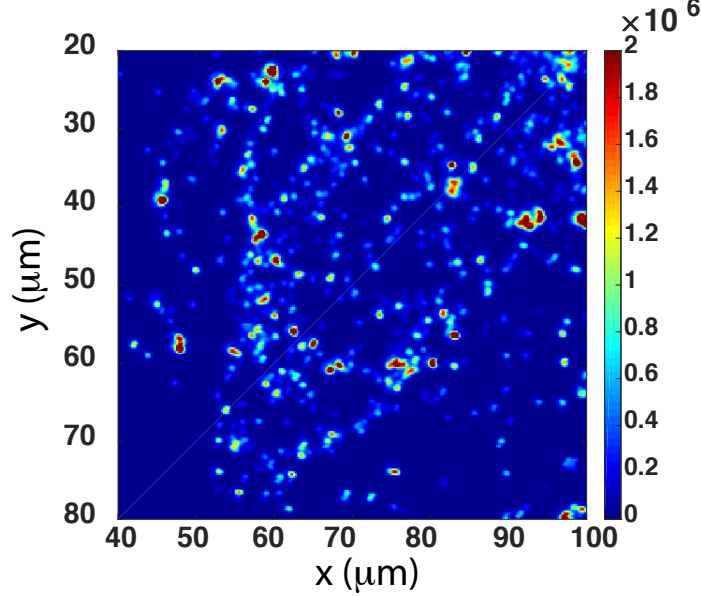


FIG. 14. Confocal map of fluorescent nano-diamonds (FND) nebulized on a quartz coverslip.

### B. Magnetic field generated by the ferromagnetic micro-particles on the attached NV centers

As mentioned in the main text, we have been able to measure the magnetic field produced by a ferromagnetic particle, while magnetized by an external field, using the nano-diamonds attached to it. To do this, both a micro-diamond containing NV centers and an hybrid particle composed of fluorescent nano-diamonds (FND) on top of a cobalt micro-particle are deposited on the ring trap electrode. We perform ESR spectrum in the presence of a magnetic field. The use of the ring trap is for us an easy way to drive the spin with microwaves.

The corresponding ESR spectra is shown in Fig. 9. For the hybrid particle, one can identify the presence of 2 FNDs. An extra 10% field is seen by the FNDs attached to the ferromagnetic particle compare to the micro-diamond alone. Depending on the position of the FND around the ferromagnet, one can expect different magnetic fields to be seen. In our measurements, the two FNDs sense the same magnetic field indicating that they are likely to be aggregated.

### C. Spin-mechanical protocol

The magnet + diamond structure will oscillate about the mean angle which will still modulate the spin-mechanical coupling. The diamond will also exert a torque to the whole structure, effectively changing the mean angle of the composite particle. For a quantum protocol with strong coupling, the mechanism is the same as outlined in [9].



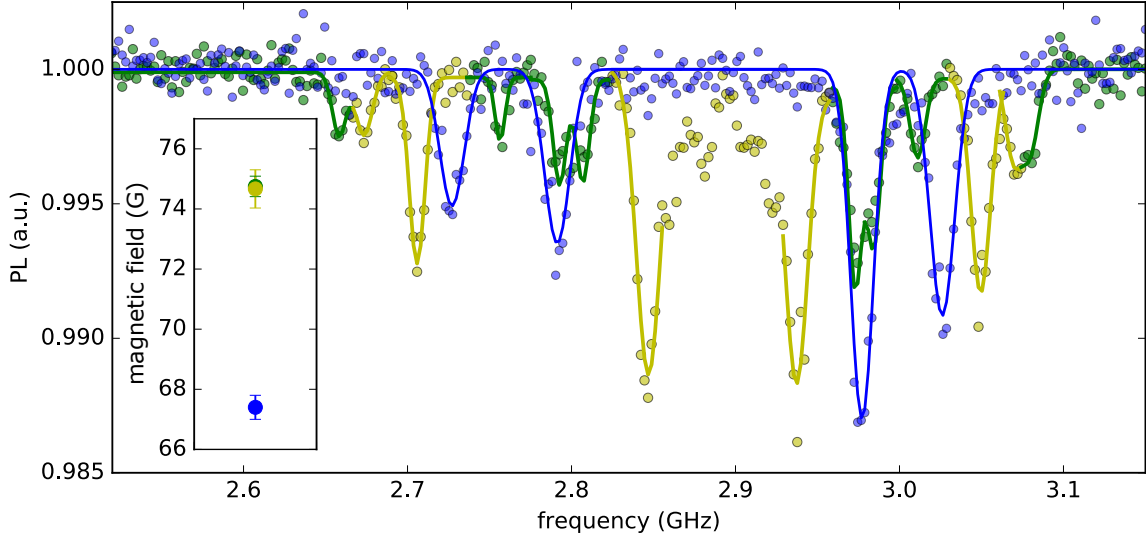


FIG. 15. Electronic Spin Resonances (ESR) scans for a micro-diamond (blue) and a hybrid particle containing 2 FNDs (green and yellow) deposited on the ring trap, at the same external magnetic field. Inset: magnetic field sensed by the different particles, determined by fitting the ESR pics positions.

The coupling strength is given by  $\lambda_\phi = \gamma B \phi_0$ , where

$$\phi_0 = \sqrt{\frac{\hbar}{2I\omega_\phi}}$$

where  $\omega_\phi$  is in turn defined by the magnetic field angle and magnitude applied at the location of the hybrid structure, i.e. by equation (2) and the inertia momentum is the one of the whole composite particle [9].

The shift of the diamond position from the center of mass (as shown in the figure 1 of the main text) will couple the center of mass and the librational modes together, but the frequency of the center of mass mode will be orders of magnitude lower so the coupling will be inefficient [10].

We estimated that with a nanodiamond and a ferromagnet both ellipsoidal with long axes of 80nm and short axis of 40 nm, a coupling of  $\lambda_\phi \sim 100\text{kHz}$  can be obtained at an external field of 30mT with an optimum angle of  $55^\circ$  [11] while the oscillator reaches a frequency of  $\omega_\phi \sim 2\pi \times 3\text{ MHz}$ .

### III. SPIN READ-OUT OF THE ANGULAR MOTION OF A LEVITATING HYBRID PARTICLE

As presented in the main text, we could perform spin read-out of a levitating particle angular motion. For this, we use a hybrid particle composed of a micro diamond (MSY 8-12 $\mu\text{m}$ ) with a 200 nm thick magnetic nickel coating on one side of the diamond. This was realized using simple sputtering of nickel atoms from an oven onto a layer of MSY cast on a quartz coverslip. The injection into the trap was done by carefully scratching the sample with a tip and the injection was done in the same manner as with the previous particles.

We stably trap the hybrid particle in the Paul trap. Applying a uniform magnetic field of around 140G then yields angular confinement of around 4.2 kHz for one of the librational mode. This mode could be parametrically excited and optically detected using the method described in the section IB. Ring down of the oscillator motion is shown in Fig. 3-e) in the main text.

To read the angular motion of the particle using the embedded NV centers spins, we exploit the angular dependency of the NVs ESR transitions frequencies. When the orientation of particle changes with respect to the external magnetic field, the frequencies of the ESR transition change and, by applying a microwave field tuned to the side of one ESR transition, so does the population in the excited spin state. Spin state population can be read out optically by collecting the NV centers Photo-Luminescence (PL) under green excitation.

Experimentally, we run the same excitation/detection sequence as for the direct detection of the particle motion, looking this time at the PL signal and applying a microwave field slightly detuned from one ESR transition. The

measurement is performed for two different microwave detunings, one on each side of the ESR transition, for which the slope of the ESR signal has an opposite sign. The corresponding ESR spectrum is shown in Fig.4-d) in the main text. Fig.17 shows the PL signal versus time after parametric excitation of the librational mode for both microwave detunings.

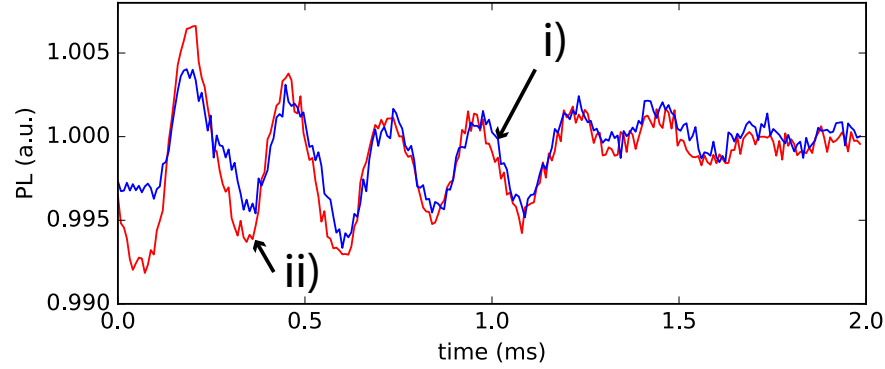


FIG. 16. Photo-luminescence signal after parametric excitation of the librational mode for positive (blue) and negative (red) detunings.

Regardless of the spin states, the amount of collected PL changes with the particle angular position. This is primarily due to the fact that the green laser illumination conditions change with the particle angular position. The PL rate thus changes when the particle rotates. Oscillations that are in phase with the particle motion are indeed clearly visible for both microwave detunings. To unambiguously extract the signal coming from the spin states, we plot the difference between the two curves. This allows to remove the spin-independent part of the signal which, again, is the same for both detunings, while keeping the spin-dependent part which has an opposite phase for both detunings.

The resulting signal is plotted in Fig.4-e) in the main text. We see that the PL signal reproduces well the direct optical measurement demonstrating a spin read-out of the particle angular motion. We note that, in our experimental conditions, direct optical measurement of the particle motion using the retro-reflected light is much more sensitive than the spin read-out. This is seen in the much better signal-to-noise ratio despite a much shorter total acquisition time for the optical (2mins) than for the spin (50mins) measurements. Interestingly however, the spin signal is slightly delayed from the optical one. This can be attributed to the finite response time of the spins population dynamics giving rise to the spins population lagging with respect to the particle motion.

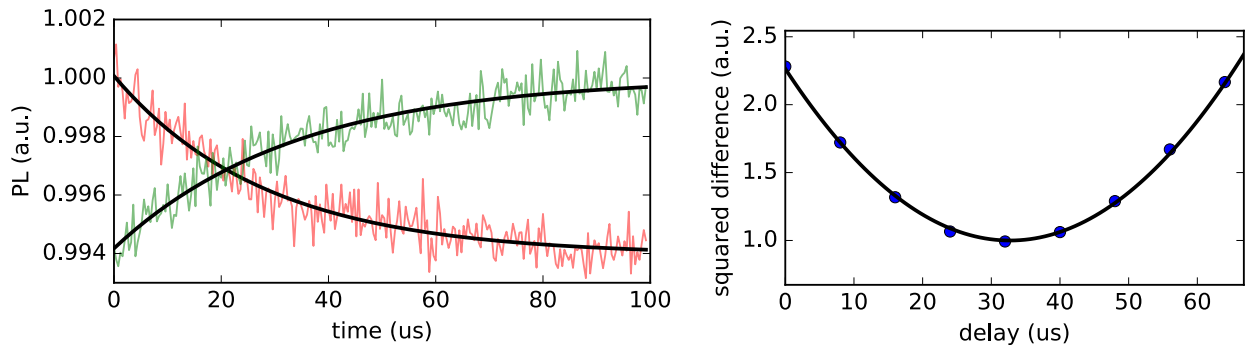


FIG. 17. Left: temporal evolution of the PL signal after switching ON (red) and switching OFF (green) a resonant microwave field. Black solid lines are exponential decay fits to the data. Right: squared difference between the spin and optical read-out of the motion for various temporal delay between them. Black solid line is a parabolic fit to the data.

To be quantitative, we plot in Fig.17 the PL count rate versus time after switching ON and OFF a resonant microwave field. This allows to measure the rate at which the spins population are excited by the microwave field and polarised by the green light. By fitting the curves with an exponential decay, we found an excitation rate of  $28\mu\text{s}$  and a polarisation rate of  $34\mu\text{s}$

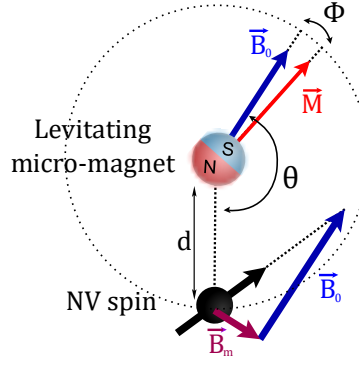


FIG. 18. Configuration of the NV center spin relative to the levitating magnet. The only degrees of freedom except  $d$  is  $\theta$  as the magnet is on average aligned with the magnetic field ( $\phi = 0$ ) and the NV center orientation is set along the total field  $\vec{B}_T$ .

Those figures can be compared to the apparent delay between the spin read-out and direct optical measurement of the particle motion. In Fig.14, we plot the squared difference between the two curves while adding a temporal delay of variable length between them. We found that the two curves coincide best for a delay of  $32\mu s$  which is in perfect agreement with the measured rate of evolution of the spins population.

#### IV. SPIN-COUPPLING BETWEEN NV CENTERS AND THE LIBRATIONAL MODE OF LEVITATING MAGNETS

Here we present the calculations involving the librational mode of levitating magnet coupled to the NV centers in details. This corresponds to the proposal b) of the Fig. 1 in the main text.

##### A. NV configuration in the field generated by the micro-magnet

As explained in the main text, the SM coupling is obtained through the field  $\vec{B}_m$  generated by the micro-magnet at the NV position. This field varies with  $\phi$ , the angle between the moment of the micro-magnet  $\vec{M}$  and its equilibrium position along the external magnetic field  $\vec{B}_0$  which can give rise to the SM coupling. To obtain a strong enough coupling, the NV center must be placed in close vicinity with the magnet (inferior to  $1\ \mu m$ ), but one can rotate the NV around the magnet and around itself.

With this regards, there are two main constraints to obtain a better coupling :

- The NV center axis must be aligned with the total magnetic field  $\vec{B}_t = \vec{B}_0 + \vec{B}_m$  to avoid spin state mixing by the transverse magnetic field. This would indeed degrade spin initialization and read-out efficiency [12].
- To enhance the SM coupling, the first order variation of  $\vec{B}_m$  in  $\phi$  should be maximal and along the NV axis.

Let us first note that the external magnetic field  $\vec{B}_0$  orientation and amplitude is already determined as we need it to confine the angular degree of freedom of the micro-magnet with a certain frequency  $\omega_\phi$ . Given a certain position of the NV center around the micro-magnet, it thus fixes the orientation of the NV axis along the total field  $\vec{B}_t$ . The only degree of freedom left is then to rotate the NV position around the magnet.

With a spherical levitating magnet, the field generated by the magnet at a point given by the polar coordinates  $(d, \theta)$  described in figure 18 will be:

$$\vec{B}_m(\theta) = \frac{MR^3}{3d^3} (2\cos(\theta - \phi)\vec{e}_r + \sin(\theta - \phi)\vec{e}_\theta) \quad (4)$$

where  $M$  is the magnetization of the magnet material,  $R$  the radius of the magnet and  $\phi$  is the angle between the magnet moment and the external field.

Since the mean orientation of the magnet is aligned with the external magnetic field  $\vec{B}_0$  (ie  $\phi = 0$ ) and the NV center is aligned along the total field  $\vec{B}_0 + \vec{B}_m$ , one can calculate the derivative of the field along the NV axis and perpendicular to it as a function of  $\theta$ .

We find that for a particular angle  $\theta_{op}$  the contribution along the NV axis is maximal and the one perpendicular to it cancels, with

$$\theta_{op} = \frac{1}{2} \arccos \left( -\frac{3B_m^0}{6B_0 + B_m^0} \right) = \arccos \sqrt{\frac{9B_0}{6B_0 + B_m^0} - 1} \quad (5)$$

where  $B_m^0 = M \frac{R^3}{d^3}$ .

At this optimal value we have  $\partial \vec{B}_t / \partial \phi = \vec{D}_\phi = B_m^0 \vec{u}_{NV}$ .

Note that this angle is actually close to  $\pi/4$  since the homogeneous magnetic field tends to be stronger at a reasonable distance from the levitating magnet.

### B. Spin-mechanical coupling scheme

In the optimum configuration the total field at the NV center is longitudinal up to the first order in  $\phi$  (see fig 1-a and SI for details). We note  $D_\phi$  its first derivative. In order to obtain a resonant SM interaction, a resonant microwave is added to drive the  $m_s = 0 \rightarrow 1$  spin transition of the NV center at a Rabi frequency  $\Omega_R = \omega_\phi$ . The spin-only part of the Hamiltonian is then diagonal in the  $|\pm\rangle = (|0\rangle \pm |1\rangle)/\sqrt{2}$  basis and the full Hamiltonian can be written :

$$\hat{H} = \omega_\phi \hat{S}_z + \gamma D_\phi \phi_0 \hat{S}_x (\hat{a}^\dagger + \hat{a}) + \omega_\phi \hat{a}^\dagger \hat{a} \quad (6)$$

where  $\hat{S}_\mu$  are the Pauli matrix operators in the  $|\pm\rangle$  basis,  $\gamma$  is the gyromagnetic ratio of the NV electron spin,  $\hat{a}^\dagger$  and  $\hat{a}$  are the creation and annihilation operators for the phonon of the angular motion, and  $\phi_0 = \sqrt{\hbar/(2I_\phi \omega_\phi)}$  its zero-point motion. This is a Jaynes-Cummings Hamiltonian and under the so-called strong coupling regime where the decoherence of both the spin and the MO are small compared to  $\lambda_\phi$ , it allows a coherent exchange between a phonon and the spin state at a rate  $\lambda_\phi$ . Combined with the ability to generate any spin state with high fidelity, one could then cool the MO to its ground state and from there generate phonon Fock states or superposition states by applying a SM pulse or engineered unitaries [13, 14].

### C. Heralding protocol to improve fidelity of phonon Fock state preparation

Once one manages to couple the spin to the librational phonons, one can use the high degree of control of the spin to generate non classical mechanical states such as Fock state (for instance the zero phonon ground state) or superposition states [13, 14]. Usual protocols are however limited by decoherence. In the case of the NV center, the limitation comes from the short  $T_2^*$ . We therefore propose a heralding of the SM interaction to improve the fidelity of Fock state generation by displacing the limit from the  $T_2^*$  to the  $T_2$ .

### D. Spin initialization and SM pulses

In order to generate an arbitrary mechanical state, one first needs to initialize the spin in the  $|+\rangle$  or  $|-\rangle$  state and then use the Jaynes-Cummings Hamiltonian to change both the spin and phonon number. The NV spin at cryogenic temperature (4K) can be initialized in the  $|0\rangle$  or  $|1\rangle$  state by using resonant optical excitation : after a number of optical cycle, the NV spin has a high probability to relax in the spin state for which the optical excitation is non-resonant. Initialization fidelity can be as high as 0.998 [15] for the  $|m_s = 1\rangle$  state. Once in the  $|m_s = 1\rangle$  state the spin can be coherently manipulated unto any superposition of the 0 and 1 state by using a microwave at the dipolar magnetic transition. One can for example go from the 0 to the  $|+\rangle$  or  $|-\rangle$  state using a  $\pi/2$ -pulse  $y$ -polarized or by adiabatically branching an  $x$ -polarized microwave. Once the spin state is initialized in the  $|+\rangle$  or  $|-\rangle$  state, a resonant  $x$ -polarized microwave is used to achieve a SM resonance between the  $|+\rangle \otimes \hat{a}|\psi\rangle$  and the  $|-\rangle \otimes |\psi\rangle$  states, where  $|\psi\rangle$  is an arbitrary mechanical state. Rabi oscillation will then occur between the two states and one can exchange a phonon with the spin states.

To cool the oscillator to the ground state, one only needs to apply a sequence of initialization/SM coupling. The fidelity of the state obtained in the stationary regime will then depends on the  $T_1$  of the oscillator and on the spin initialization and SM interaction efficiency.

Once in the ground state, one can generate arbitrary states by applying a sequence of initialization followed by a controlled pulse. To obtain a high fidelity, one is however limited to the strong coupling regime as the decoherence will damp the Rabi oscillation and in fact results in imperfect SM pulses.

### E. Limitation caused by decoherences sources

Since the scheme does not requires shining light on the levitating magnet the main mechanical decoherence is expected to come from gas collision with the levitating particle. The decoherence of the mechanical oscillator will limit the time during which the whole experiment sequence (cooling, mechanical state preparation, measurement) can be carried out. Although some theoretical tool are being developed to estimate the decoherence rate [16, 17] of librational states, it will highly depends on the shape of the levitating particle, its roughness and eventually the potential governing the scattering of molecules impacting it. Note that it can be strongly mitigated if one works with an isotropic particle [16, 17] or at high enough vacuum. To give a rough estimate of the heating rate and hence of the lifetime of a mechanical state, we calculate the damping rate of the levitating particle  $\Gamma_{gas}$  due to air molecules in the classical regime.

In the Knudsen regime, when the mean free path of the gas molecule is higher than the size of the levitating particle, one gets [18] :

$$\Gamma_{gas} = \sigma_{eff} \frac{10\pi P}{a\rho \bar{c}} \quad (7)$$

with  $\sigma_{eff} \sim 1.1$  the accommodation coefficient,  $a$  the radius of the particle,  $P$  the pressure in Pa,  $\rho$  its density and  $\bar{c}$  the molecular velocity of the gas molecules considered. We obtain a relatively low heating rate : for a  $1\mu m$  radius sphere  $eg$  it is of about 1Hz at  $P = 10^{-3}$ mbar.

The NV spin itself has an excellent lifetime at cryogenic temperature, up to a hundred seconds which is not limiting [19]. However NV spins are coupled to the fluctuating nuclear spin bath of the diamond crystal. This results in fluctuations of the frequency of the NV spin and considerably reduces the  $T_2^*$ . Although this effect can be mitigated by using isotopically purified diamond to remove  $^{13}C$  spins [20, 21], the best linewidth as far as we know was as low as 2 kHz [22].

### F. Imperfect $\pi$ pulse and Spin-cooling

With a SM coupling faster than the lifetimes but smaller than  $1/T_2^*$ , the result will be imperfect coherent control of the system. Let us consider a SM sequence with a SM interaction time calibrated to produce a  $\pi$ -pulse for a resonant interaction. Depending on the state of the spin bath the spin-mechanical system will be detuned from the resonance and the SM pulse will result in a coherent superposition of  $|+\rangle \otimes \hat{a}|\psi\rangle$  the  $|-\rangle \otimes |\psi\rangle$  states where  $|\psi\rangle$  is an arbitrary mechanical state. The proportion of the superposition will depend on the detuning and the coupling strength, the result is therefore a statistical mixture of coherent superposition of entangled states.

As long as  $\lambda_\phi$  is not negligible compared to  $1/T_2^*$ , cooling to the ground state is still possible as the spin-phonon exchange efficiency will not drop much below 50%. The fidelity of the ground state obtained in the stationary state of a cooling sequence can still be high if the heating rate (or  $T_1$  of the oscillator) is low enough. For example, if one takes a simplified model that includes only the ground and the 1-phonon Fock state, the stationary population  $\sigma_1^s$  in the 1-phonon Fock state reads

$$\sigma_1^s = \frac{\Gamma_h}{\Gamma_h + \Gamma_c} \quad (8)$$

where  $\Gamma_h = \Gamma_{gas}$  and  $\Gamma_c \sim \lambda_\phi$ . At a pressure  $P = 6.10^{-3}$ mbar, we will have a mean phonon number  $n^s \sim \sigma_1^s = 0.05$  and at  $P = 2.10^{-4}$ mbar we will have  $n^s < 0.002$  with  $\sigma_1^s$  not limited by gas heating but by the fidelity of the initialization of the spin state.

### Spin read-out and Heralding protocol

When generating a Fock state, one can increase the fidelity which was lost due to decoherence by measuring the spin state after the SM coupling, therefore heralding the spin-phonon exchange. As stated above, after an imperfect SM pulse, one obtain a superposition of entangled state which population varies statistically and which we don't know. If one then read-out the spin state, a quantum jumps occurs and the mechanical state is projected onto one of the two SM entangled states  $|+ \rangle \otimes \hat{a}|\psi \rangle$  and  $|-\rangle \otimes |\psi \rangle$ . This allows one to repeat the SM coupling sequence in the case the spin state has not changed, thus increasing the fidelity of such state preparation.



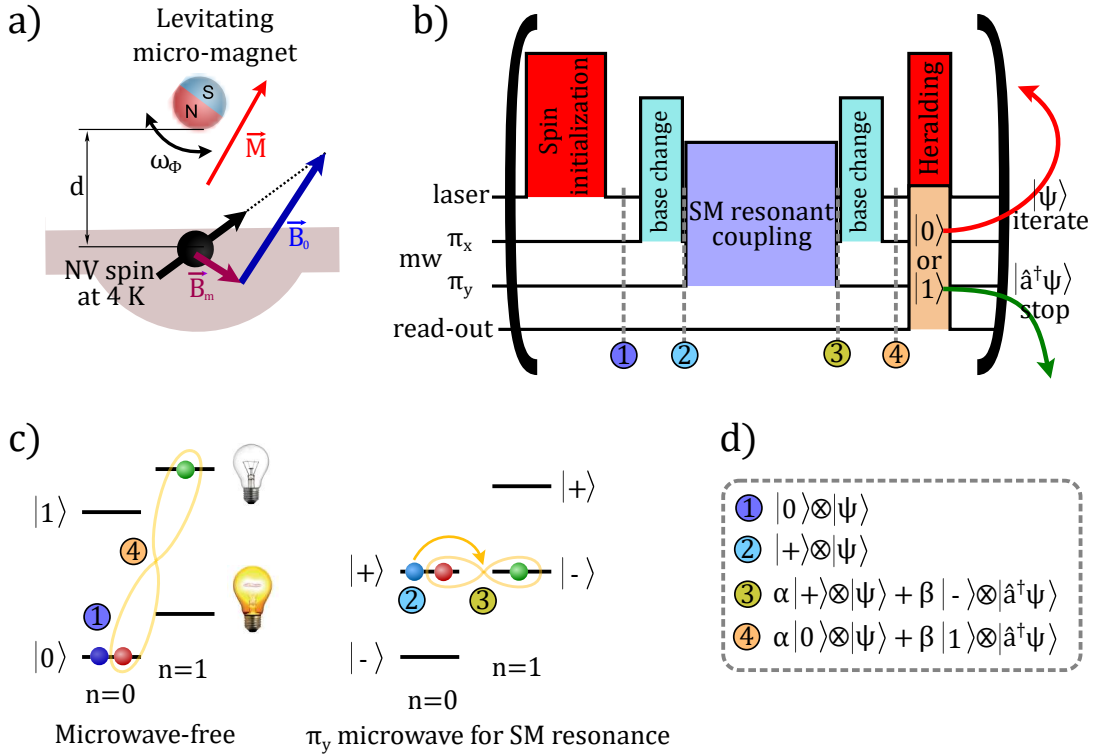


FIG. 19. a) Experimental scheme proposed : a magnet is levitated at a distance  $d$  from an NV spin within a bulk diamond at cryogenic temperature. (b) Sequence for heralded generation of a Fock state.  $|\Psi\rangle$  is an arbitrary mechanical state, for instance the ground state. (c) Level diagram for the hybrid SM system with and without microwave. Colored points show the populated levels during a sequence for creating a 1 phonon Fock state from the ground state. Here  $|\psi\rangle$  is the  $n = 0$  phonon state. (d) State of the hybrid system during a sequence that increases the phonon number by one.

High fidelity read-out of the NV spin state can be achieved using resonant optical excitation of the dipolar transition. Since the optical transition at cryogenic temperature is non degenerated for the 0 and 1 spin state, the presence or absence of photoluminescence after a resonant excitation on one of the transition allows one to deduce the spin state. Using this technique, fidelity as high as 0.96 has been achieved [23] and might still be improved by collecting even more photons from the NV center or reducing the dark count.

The protocol for a heralded SM interaction is described in figure 19. First, the spin is prepared in the desired state (states labeled 1 and 2 in the figure 19) using a combination of optical and microwave pulses, then the resonant coupling is turned on for a duration sufficient to transfer non negligible populations. Then the  $+$  and  $-$  states are mapped onto the 0 and 1 state and the spin states are optically read-out. If the SM interaction has failed after collapsing the SM-entangled state (*ie* the spin state has not changed), the sequence is repeated until it is successful. For low phonon Fock state, one can maximize the fidelity at the expense of time by adding a cooling step at the beginning of each iteration and restarting from the ground state.

Note that such protocols only allow generation of Fock states. Generating a given superposition state with high fidelity would still require the strong coupling regime to be attained or using more involved protocols. One should also note that the full protocol is simplified here : with the protocol described above, the  $T_2^*$  will induce an error while mapping the  $|+\rangle$  state onto the  $|0\rangle$  state. Standard spin-echo methods can however be used to remove this error.

### Fidelity for one phonon Fock state generation

The fidelity of the state generated after a heralded spin-phonon coupling can be easily calculated for the one phonon Fock state. Let us consider  $\eta$  the probability of having generated a one phonon Fock state after one iteration of the spin mechanical coupling sequence, before measurement.  $\eta$  depends on the coupling strength  $\lambda_\phi$ , on the dephasing time  $T_2^*$ , on the spin initialization fidelity and on the fidelity of the cooled state. We note  $F_1$  the read-out fidelity on the spin state. Because we perform projective read-out of the spin state, the fidelity of the state after read-out can

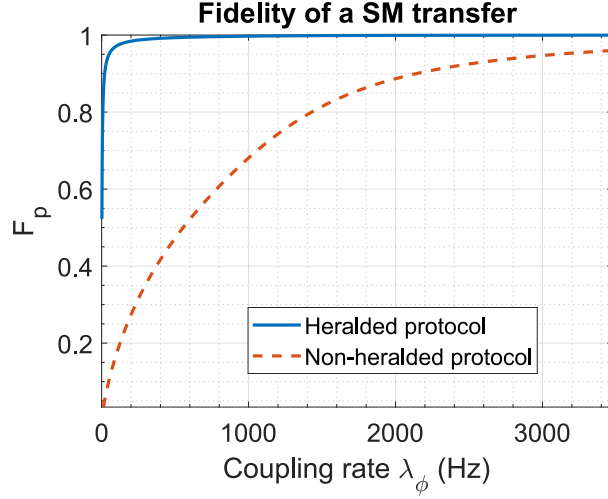


FIG. 20. Fidelity for the preparation of a one phonon Fock state from the ground state with a heralded (continuous line) and non-heralded (dotted line) protocol. The spin-mechanical interaction time is chosen in order to obtain a  $\pi$  pulse at resonance.

simply be calculated from a conditional probability calculus and reads

$$F_p = \frac{\eta F_1}{(1 - F_1(1 - \eta) + \eta F_1)}. \quad (9)$$

Note that here both the spin and phonon states are re-initialized after each failed iteration. Although time lost to generate a one phonon state is low, it will increase exponentially with the phonon number we want to generate.

### Fidelity for arbitrary Fock state generation

Here we calculate the probability to successfully transfer the MO from one Fock state to another one with adjacent phonon number. We consider the iterated sequence described in the precedent section. Here we propose not to reinitialize the phonon state after the sequence has failed, yielding a lower averaged fidelity, but to increase the interaction time linearly with the phonon number to generate. We calculate the average fidelity of the sequence, *i.e.* the fidelity of the generated state, if increases by one unit the phonon number, starting with a Fock state. We consider two major errors which could make the sequence fail :

- The finite  $T_1$  time, which makes the spin or the oscillator changes state during the sequence
- Errors in read-out or initialization : the state of the spin is wrongfully initialized or read-out

The  $T_1$  of the spin and of the MO simply adds a factor  $P_{T_1} = \exp(-T_s(1/T_1^{NV} + 1/T_1^{MO}))$  to the fidelity for each iteration of a sequence which lasts  $T_s$ .

For the other source of errors, we estimate the probability for the sequence not to fail, which means either successfully exchanging a phonon state with the spin while confirming it ( $P_{succ}^{stop}$ ), or successfully measuring the failure of the SM interaction while both the spin and the MO remained unaltered ( $P_{unalt}^{iter}$ ). Here, we neglect the probability of two errors correcting themselves to give the expected results and therefore slightly underestimate the success probability.

The success probability  $P_{success}$  can then be written :

$$P_{success} = P_{succ}^{stop} + P_{unalt}^{iter} \times P_{success} \quad (10)$$

$$= P_{succ}^{stop} / (1 - P_{unalt}^{iter}) \quad (11)$$

The spin initialization and read-out fidelities for the 0 and 1 spin are noted  $F_w$  and  $F_{0/1}$  respectively. The probability of SM transfer, in fact the probability to go from one Fock state to the other by employing a SM  $\pi$  pulse is finally noted  $P_{tr}$  and depends on  $\lambda_\phi$  and  $T_2^*$ . We then have :

$$P_{succ}^{stop} = F_w \times P_{tr} \times P_{T_1} F_1 \quad (12)$$

$$P_{unalt}^{iter} = [F_w \times (1 - P_{tr}) \times F_0 + (1 - F_w) \times (1 - P_{tr})] \times P_{T_1} \quad (13)$$

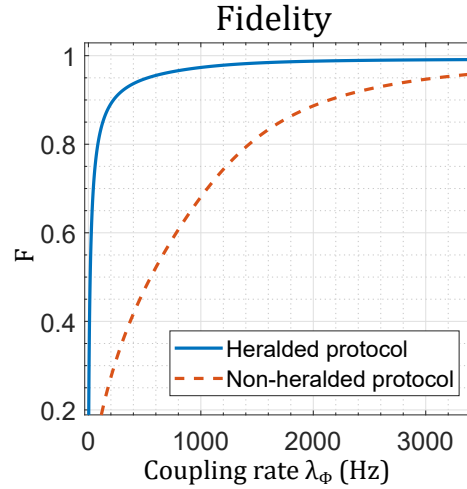


FIG. 21. Fidelity for the preparation of a one phonon Fock state from the ground state with a heralded (continuous line) and non-heralded (dotted line) protocol.

The fidelity can then be plotted as a function of  $\lambda_\phi$  as in figure 21. One can see the error is considerably reduced by the heralding protocol compared with  $P_{tr}$ , obtained with no heralding scheme. When  $\lambda_\phi$  and  $P_{tr}$  drops, the main limitation then comes from the number of iteration that are necessary in average while the errors on spin read-out and initialization are accumulated.

- 
- [1] T. Delord, L. Nicolas, L. Schwab, and G. Hétet, New Journal of Physics **19**, 033031 (2017).
  - [2] T. Delord, L. Nicolas, M. Bodini, and G. Hétet, Applied Physics Letters **111**, 013101 (2017).
  - [3] T. Delord, P. Huillery, L. Schwab, L. Nicolas, L. Lecordier, and G. Hétet, Phys. Rev. Lett. **121**, 053602 (2018), URL <https://link.aps.org/doi/10.1103/PhysRevLett.121.053602>.
  - [4] H. Straubel, Naturwissenschaften **42**, 506 (1955), ISSN 1432-1904, URL <https://doi.org/10.1007/BF00601196>.
  - [5] N. Yu, W. Nagourney, and H. Dehmelt, Journal of Applied Physics **69**, 3779 (1991).
  - [6] J. J. Abbott, O. Ergeneman, M. P. Kummer, A. M. Hirt, and B. J. Nelson, IEEE Transactions on Robotics **23**, 1247 (2007), ISSN 1552-3098.
  - [7] J. A. Osborn, Phys. Rev. **67**, 351 (1945), URL <https://link.aps.org/doi/10.1103/PhysRev.67.351>.
  - [8] L. Rondin, J.-P. Tetienne, T. Hingant, J.-F. Roch, P. Maletinsky, and V. Jacques, Reports on Progress in Physics **77**, 056503 (2014).
  - [9] T. Delord, L. Nicolas, Y. Chassagneux, and G. Hétet, Phys. Rev. A **96**, 063810 (2017).
  - [10] S. Liu, T. Li, and Z. qi Yin, J. Opt. Soc. Am. B **34**, C8 (2017), URL <http://josab.osa.org/abstract.cfm?URI=josab-34-6-C8>.
  - [11] Y. Ma, T. M. Hoang, M. Gong, T. Li, and Z.-q. Yin, Phys. Rev. A **96**, 023827 (2017).
  - [12] J.-P. Tetienne, L. Rondin, P. Spinicelli, M. Chipaux, T. Debuisschert, J.-F. Roch, and V. Jacques, New Journal of Physics **14**, 103033 (2012).
  - [13] P. Rabl, P. Cappellaro, M. V. G. Dutt, L. Jiang, J. R. Maze, and M. D. Lukin, Phys. Rev. B **79**, 041302 (2009), URL <https://link.aps.org/doi/10.1103/PhysRevB.79.041302>.
  - [14] C. Law and J. Eberly, Physical review letters **76**, 1055 (1996).
  - [15] B. Hensen, H. Bernien, A. E. Dréau, A. Reiserer, N. Kalb, M. S. Blok, J. Ruitenbergh, R. F. Vermeulen, R. N. Schouten, C. Abellán, et al., Nature **526**, 682 (2015).
  - [16] B. A. Stickler, B. Papendell, and K. Hornberger, Physical Review A **94**, 033828 (2016).
  - [17] C. Zhong and F. Robicheaux, Physical Review A **94**, 052109 (2016).
  - [18] J. Fremerey, Vacuum **32**, 685 (1982).
  - [19] A. Jarmola, V. M. Acosta, K. Jensen, S. Chemerisov, and D. Budker, Phys. Rev. Lett. **108**, 197601 (2012).
  - [20] N. Mizuochi, P. Neumann, F. Rempp, J. Beck, V. Jacques, P. Siyushev, K. Nakamura, D. Twitchen, H. Watanabe, S. Yamasaki, et al., Physical review B **80**, 041201 (2009).
  - [21] G. Balasubramanian, P. Neumann, D. Twitchen, M. Markham, R. Kolesov, N. Mizuochi, J. Isoya, J. Achard, J. Beck, J. Tissler, et al., Nature materials **8**, 383 (2009).
  - [22] P. C. Maurer, G. Kucsko, C. Latta, L. Jiang, N. Y. Yao, S. D. Bennett, F. Pastawski, D. Hunger, N. Chisholm, M. Markham, et al., Science **336**, 1283 (2012), ISSN 0036-8075, <http://science.sciencemag.org/content/336/6086/1283.full.pdf>, URL

<http://science.sciencemag.org/content/336/6086/1283>.

- [23] P. C. Humphreys, N. Kalb, J. P. Morits, R. N. Schouten, R. F. Vermeulen, D. J. Twitchen, M. Markham, and R. Hanson, *Nature* **558**, 268 (2018).
-